Optics Letters

Turn-key, high-efficiency Kerr comb source

Bok Young Kim,[1,*] Yoshitomo Okawachi,[1] Jae K. Jang,[1] Mengjie Yu,[1,5] Xingchen Ji,[2,3] Yun Zhao,[2] Chaitanya Joshi,[1,4] Michal Lipson,[1,2] and Alexander L. Gaeta[1,2]

[1]Department of Applied Physics and Applied Mathematics, Columbia University, New York, New York 10027, USA
[2]Department of Electrical Engineering, Columbia University, New York, New York 10027, USA
[3]School of Electrical and Computer Engineering, Cornell University, Ithaca, New York 14853, USA
[4]School of Applied and Engineering Physics, Cornell University, Ithaca, New York 14853, USA
[5]Current address: John A. Paulson School of Engineering and Applied Sciences, Harvard University, Cambridge, Massachusetts 02138, USA
*Corresponding author: bokyoung.kim@columbia.edu

Received 12 July 2019; revised 18 August 2019; accepted 19 August 2019; posted 20 August 2019 (Doc. ID 372439); published 6 September 2019

We demonstrate an approach for automated Kerr comb generation in the normal group-velocity dispersion (GVD) regime. Using a coupled-ring geometry in silicon nitride, we precisely control the wavelength location and splitting strength of avoided mode crossings to generate low-noise frequency combs with pump-to-comb conversion efficiencies of up to 41%, which is the highest reported to date for normal-GVD Kerr combs. Our technique enables on-demand generation of a high-power comb source for applications such as wavelength-division multiplexing in optical communications.

https://doi.org/10.1364/OL.44.004475

Comb generation in microresonators enables integrated and robust platforms [1,2] that can be used for numerous applications such as spectroscopy [3–6], distance ranging [7,8], frequency synthesis [9,10], optical clocks [11], and data communications [12,13]. Recently, significant progress has been made in integrating microresonator combs by using low-power, electrically pumped sources [14–16], and by utilizing novel generation methods such as pump modulation [17,18] or thermal control of the resonances [19]. These platforms operate in the anomalous group-velocity dispersion (GVD) regime, where dissipative cavity solitons are formed [20]. However, Kerr combs operating in the single-soliton regime have a low pump-to-comb conversion efficiency [21]. A normal-GVD comb, on the other hand, readily offers high conversion efficiencies and exhibits a slower spectral power falloff [21,22]. Normal-GVD combs can be generated through pump modulation at the microresonator free spectral range (FSR) [23] or more commonly by exploiting the coupling between different mode families [22,24–28]. Although different mode families possess different frequency mode spacings, it is possible for modes in two different families to spectrally overlap and couple to each other, leading to a mode splitting at the degeneracy point [29,30]. Such an avoided mode crossing effectively creates a local region of anomalous GVD and enables the generation of modulation instability (MI) sidebands [28], which is known to be crucial to the initial generation dynamics of a comb [31].

All previous demonstrations of normal-GVD combs have the disadvantage of requiring tuning the frequency of the pump laser near the mode crossing point. Compared to fixed-frequency lasers, tunable lasers typically have relatively broader linewidths on the order of 100 kHz, which in turn, determines the linewidth of the comb lines. They also have a long-term frequency drift that shifts the center wavelength and limits the stability of the generated comb [19]. Depending on device parameters, the required mode interaction (e.g., coupling to higher order modes) may occur at an undesirable wavelength that could cause non-native comb line spacing [26] or even inhibit comb generation. To overcome these limitations, a tunable mode interaction should be implemented with a fixed-frequency laser. This would allow for straightforward automation of the comb generation process, thereby establishing the path to a fully integrated, turn-key microresonator comb system.

In this Letter, we report the first demonstration of microresonator frequency comb generation in the normal-GVD regime using a fixed-frequency laser source. An avoided crossing is introduced using a coupled-ring geometry, and its wavelength location and splitting strength are precisely controlled with integrated heaters. Such control over the mode crossing allows for straightforward use of a computer-controlled system to generate a high-efficiency (41%) Kerr frequency comb. We show that our system is insensitive to the tuning speed in contrast to soliton generation [19]. Finally, we investigate the noise and coherence of the generated comb and determine the conditions for exciting a comb with high coherence.

As shown in Fig. 1(a), our oxide-clad silicon nitride (SiN) device utilizes coupled-ring resonators (main and auxiliary) with integrated platinum resistive heaters. Each microresonator has a waveguide cross section of 730 × 1000 nm, which allows for the fundamental TE polarization mode to be in the normal-GVD regime near the pump wavelength. The loaded Q factor of the main ring resonator is measured to be 5×10^5. An important factor that impacts the comb bandwidth is the strength of the mode coupling. For our normal-GVD comb, an avoided mode crossing is required near the pump wavelength without additional mode interactions elsewhere. Therefore, we exploit the Vernier effect [32] and design the device to have mode

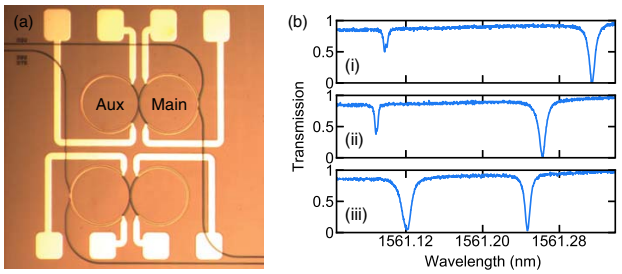

Fig. 1. (a) Image of two devices, each consisting of two coupled-ring resonators with integrated platinum resistive heaters. (b) Transmission of device using a counterpropagating probe 1 FSR away from the pump wavelength (1559.79 nm). Split resonances (i) as the main ring heater is tuned, (ii) before parametric oscillation, and (iii) during comb generation.

interactions every 50 nm by slightly offsetting the FSRs of each microresonator from one another. The main ring has an FSR of 200 GHz while the auxiliary ring has an FSR of 206 GHz. The coupling gap between the main ring and the auxiliary ring is 525 nm, which leads to a mode splitting of 7.1 GHz. To enable high pump-to-comb conversion efficiency, we operate in the overcoupled regime [33] using a bus to main ring gap of 525 nm.

In our experiments, a computer controls an arbitrary waveform generator and individually tunes the resonances of our coupled SiN ring resonators. A thermoelectric cooler is employed for consistent day-to-day operation. A narrow linewidth (1 kHz), continuous-wave (CW) fixed-frequency laser at 1559.79 nm [dense wavelength-division multiplexing (DWDM) ITU channel 22] is used as the pump source. The laser light is amplified with an erbium-doped fiber amplifier, and 180 mW of power is coupled into the bus waveguide using a lensed fiber. The free-space output from the device is collimated using an aspheric lens and coupled to a fiber using a collimator. The output is split 80:20 and is collected for analysis by an optical spectrum analyzer (OSA) and an electrical spectrum analyzer, respectively.

Normal-GVD comb generation is initiated by satisfying the phase-matching and power threshold requirements for intracavity MI [28]. In our system of induced mode interactions, pumping the redshifted resonance at a mode splitting satisfies the phase-matching requirement. A local alteration of the GVD occurs where there is effectively anomalous GVD between the redshifted resonance and the primary MI sideband modes. However, due to the strong interaction between the microresonators, pumping at the exact crossing results in large loss, and the power threshold requirements cannot be satisfied. To overcome this loss, nearby resonator modes can be pumped since adequate mode splitting is still present but with reduced loss [32]. In order to maximize intracavity power while pumping the redshifted resonance at a splitting, the lower wavelength adjacent resonator mode is pumped. Our generation scheme relies on the ability to control the wavelength location and the strength of the mode splitting. By increasing the electrical power through the integrated heaters on our device, the resonances of the microresonators can be thermally redshifted by more than one FSR [19]. Therefore, the mode splitting can be tuned by shifting the frequency degeneracy of the two mode families. Redshifting the smaller (larger) FSR mode family resonances redshifts (blueshifts) the mode crossing. In our method, a main ring resonance is blue-detuned towards the pump wavelength λ_p. However, the blueshifting of the main ring (smaller FSR mode family) resonances is accompanied by the blueshifting of the degeneracy point. To account for this effect, the degeneracy is positioned at a higher wavelength than λ_p by a few resonator modes [(i) and (ii) in Fig. 1(b)]. After the heater powers are set accordingly, the main ring resonance is blueshifted towards λ_p along with the degeneracy wavelength. Intracavity power builds up, leading to a temperature increase in the cavity that offsets the temperature reduction due to the decrease in heater power. Once the intracavity power is large enough, the decrease in heater power does not shift the split resonances [(iii) in Fig. 1(b)].

Figure 2 shows the evolution of our normal-GVD comb for part of the computer-controlled process where the electrical power to the main ring heater is tuned from 28 to 16 mW while the auxiliary ring is set to a constant 82 mW.

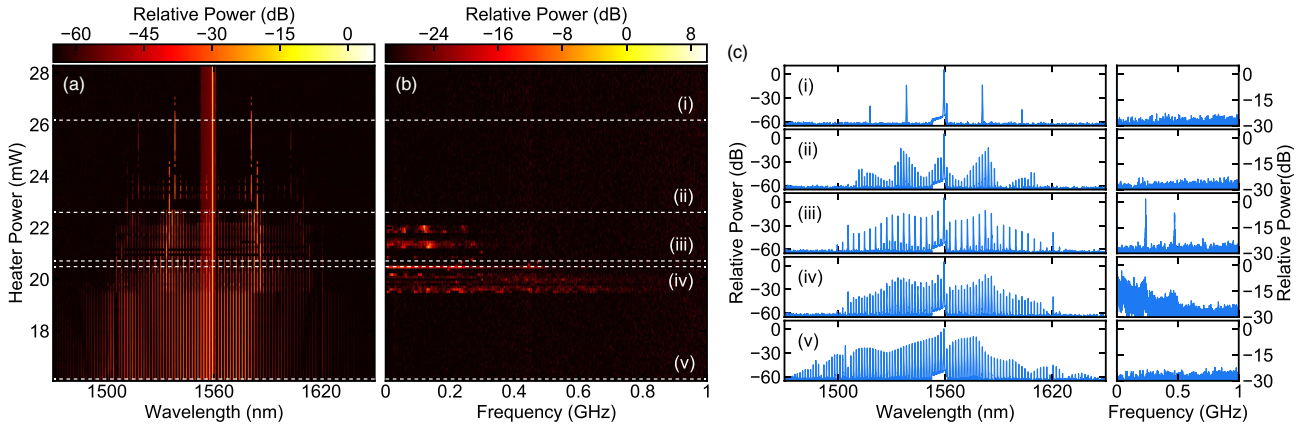

Fig. 2. (a) Measured comb spectra and (b) corresponding RF noise spectra for different cavity resonance detunings during the automated process. The power in the main ring heater is tuned from 28 to 16 mW while that of the auxiliary ring is set at 82 mW. (c) Optical and RF spectra at heater powers indicated by dashed lines are shown in (a) and (b). The small peak observed 1 FSR away from the pump wavelength is due to the reflection of a counterpropagating probe used to observe the mode splitting during the process. (i) Initial sideband generation from intracavity MI. (ii) Initial filling in of comb lines. (iii) Multicomb state with sharp noise peaks. (iv) Broadband high-noise comb state. (v) Final low-noise comb state with a high pump-to-comb conversion efficiency.

These power values were obtained by performing a thorough characterization of the device, which also accounts for the thermal cross talk between the heaters, before using the device for deterministic comb operation. As intracavity power begins to grow, primary sidebands due to MI are formed, and the characteristic low radio frequency (RF) noise of the process is observed [(i) in Fig. 2(c)]. The comb then begins to fill in as the resonance is tuned further towards λ_p [(ii) in Fig. 2(c)]. The primary sidebands then grow and serve as pump fields that generate separate combs and induce sharp peaks in the RF spectrum [(iii) in Fig. 2(c)]. Tuning further into the resonance, we see a broadband high-noise state [(iv) in Fig. 2(c)]. The rise in RF noise is attributed to the broadband MI gain from the two strong primary sidebands serving as pump fields [34]. As the power in the cavity increases, noise is generated from spontaneous four-wave mixing. Finally, as the resonance is further blue-detuned, we observe a sharp drop in noise [(v) in Fig. 2(c)], and the comb is phase-locked while maintaining a high pump-to-comb conversion efficiency. A key reason our method for comb generation can be automated is that the desired comb state persists over a large heater tuning range from 20 to 16 mW [Fig. 2(a)]. In contrast to conditions required for the soliton state, where the heater scan speed must be close to the thermal time constant of the ring to counter the thermal recoil [19], the large detuning range in our system allows for arbitrary heater scan speeds to consistently reach the low-noise comb state.

The RF noise is directly correlated to the coherence of the comb. We measure the coherence by using the technique given in [35]. For this setup, we use a fiber-based asymmetric Mach–Zehnder interferometer to overlap the output sampled at two different times and create spectral fringes from their relative time delay. The path-length difference is set to 3 m, which corresponds to a few photon lifetimes and a linewidth resolution of 100 MHz. Such a laser linewidth is sufficient for digital modulation applications such as differential phase-shift keying. Utilizing the instability of the interferometer, we obtain 50 OSA traces to measure the visibility of these spectral fringes. The visibility at wavelength λ is given by

$$V(\lambda) = \frac{I_{\max}(\lambda) - I_{\min}(\lambda)}{I_{\max}(\lambda) + I_{\min}(\lambda)}, \tag{1}$$

where $I_{\max}(\lambda)$ and $I_{\min}(\lambda)$ are the maximum and minimum intensities at λ, respectively. The resulting coherence is

$$|g_{12}^{(1)}(\lambda)| = \frac{I_1(\lambda) + I_2(\lambda)}{2\sqrt{I_1(\lambda) I_2(\lambda)}} V(\lambda), \tag{2}$$

where $I_1(\lambda)$ and $I_2(\lambda)$ are the intensities in each arm of the interferometer [36]. After calibrating for power differences in the arms, we show that the relevant lines of the generated comb are highly coherent with a minimum coherence of 94% [Fig. 3(a)]. We also measure the coherence of the comb in a high-noise state. Figure 3(b) shows the calculated coherence for the high-noise comb state, and we observe, as expected, that aside from the pump line, the comb lines show low coherence.

We examine the pump-to-comb conversion efficiency, which is defined to be the ratio between the power of all the comb lines sans the pump line and the pump power in the bus waveguide. For the generated spectrum shown in Fig. 4, the comb line spacing is 201.6 GHz, and the conversion efficiency is measured to be 40.6%. Figure 4 shows 18 lines with powers greater than 1 mW, 38 lines with powers greater than 100 μW,

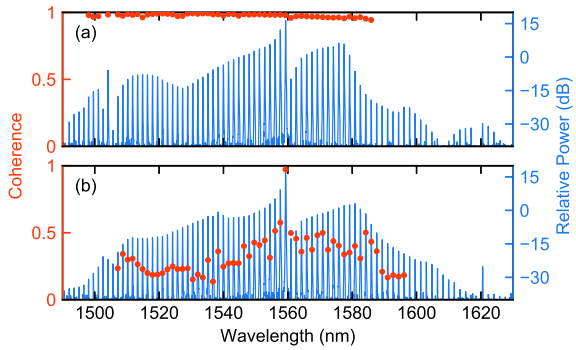

Fig. 3. Coherence measurement of (a) low-noise comb state with high pump-to-comb conversion efficiency, and (b) high-noise comb state.

and 51 lines with powers greater than 50 μW. The 51 comb lines occur sequentially in mode number between 1495 and 1583 nm except for the three modes lying between 1505 and 1509 nm. These three comb lines are weaker in power due to the periodicity of the induced avoided mode crossing. Similar depletion of comb line powers can be observed one higher comb mode from the pump and near 1619 nm. Therefore, increasing the frequency separation between mode interactions would eliminate such depletions of comb line powers and potentially broaden the comb. The comb bandwidth can also be increased by reducing the GVD through dispersion engineering and by increasing the mode splitting [28]. In the normal-GVD regime, the FSR of a resonator decreases with frequency. As a result, the phase-matched MI process will occur at more distant modes if the magnitude in FSR change is reduced through the reduction in GVD. Likewise, increasing the mode splitting will allow for greater compensation of the GVD and broaden the comb.

Lastly, we show that the automated method applies generally across other configurations for the coupled-ring geometry. Figure 5(a) shows the spectrum when the coupling gap between the rings is 475 nm, which corresponds to a stronger mode interaction. Other devices were also tested that generated similar spectra, indicating this method is not limited to one device. Returning to the original device, Fig. 5(b) shows the spectrum when the pump was set to 115 mW. Similar spectra were generated for a range of pump powers from 115 to 200 mW. Figure 5(c) shows the spectrum when the pump wavelength is set at 1540.56 nm (DWDM ITU channel 46) by a narrow

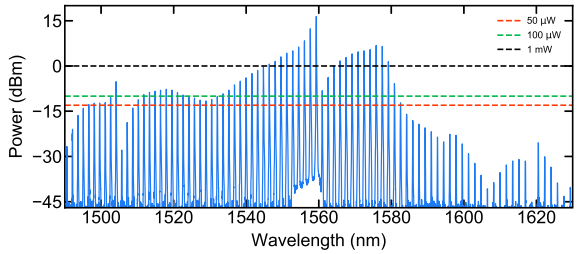

Fig. 4. Measured comb spectrum from automated generation with a comb line spacing of 201.6 GHz and a 41% pump-to-comb conversion efficiency. Power levels of 50 μW, 100 μW, and 1 mW are given by red, green, and black dashed lines, respectively. There are 18 lines with powers greater than 1 mW, 38 lines with powers greater than 100 μW, and 51 lines with powers greater than 50 μW.

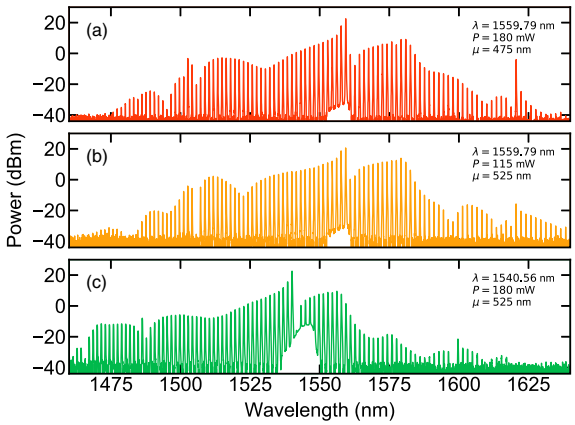

Fig. 5. Measured comb spectra from automated generation in different configurations for the coupled-ring geometry. (a), (b) Pump wavelength set at 1559.79 nm. (a) Pump power set at 180 mW with 475 nm coupling gap between main and auxiliary ring. (b) Pump power set at 115 mW with 525 nm coupling gap. (c) Pump wavelength set at 1540.56 nm and pump power set at 180 mW with 525 nm coupling gap.

linewidth (1 kHz), CW fixed-frequency laser. We have also used a tunable CW laser to set different pump wavelengths and successfully generated the final comb state.

In conclusion, we have demonstrated a systematic approach to generating high-power Kerr combs using a fixed-frequency laser source. Our technique increases the stability of a comb and can overcome variations in the parameter settings arising from minute differences in fabrication. The on-demand generation method produces low-noise and high-power comb lines that are useful for applications such as communications by eliminating the need for multiple laser sources. Furthermore, high-power combs are useful in other areas such as spectroscopy, where the detection of power in each comb line is critical. By automating the generation scheme, we have shown that turn-key operation is a reality for such microresonator frequency comb systems.

Funding. Advanced Research Projects Agency—Energy (DE-AR0000843); Air Force Office of Scientific Research (FA9550-15-1-0303); National Science Foundation (NSF) (ECS-0335765); Small Business Innovation Research (FA8650-19-C-1002).

Acknowledgment. This work was performed in part at the Cornell NanoScale Facility, a member of the National Nanotechnology Infrastructure Network, which is supported by the NSF.

REFERENCES

1. T. J. Kippenberg, A. L. Gaeta, M. Lipson, and M. L. Gorodetsky, Science **361**, eaan8083 (2018).
2. A. L. Gaeta, M. Lipson, and T. J. Kippenberg, Nat. Photonics **13**, 158 (2019).
3. M.-G. Suh, Q.-F. Yang, K. Y. Yang, X. Yi, and K. J. Vahala, Science **354**, 600 (2016).
4. M. Yu, Y. Okawachi, A. G. Griffith, M. Lipson, and A. L. Gaeta, Opt. Lett. **42**, 4442 (2017).
5. M. Yu, Y. Okawachi, A. G. Griffith, N. Picqué, M. Lipson, and A. L. Gaeta, Nat. Commun. **9**, 1869 (2018).
6. A. Dutt, C. Joshi, X. Ji, J. Cardenas, Y. Okawachi, K. Luke, A. L. Gaeta, and M. Lipson, Sci. Adv. **4**, e1701858 (2018).
7. M.-G. Suh and K. J. Vahala, Science **359**, 884 (2018).
8. P. Trocha, M. Karpov, D. Ganin, M. H. P. Pfeiffer, A. Kordts, S. Wolf, J. Krockenberger, P. Marin-Palomo, C. Weimann, S. Randel, W. Freude, T. J. Kippenberg, and C. Koos, Science **359**, 887 (2018).
9. W. Liang, D. Eliyahu, V. S. Ilchenko, A. A. Savchenkov, A. B. Matsko, D. Seidel, and L. Maleki, Nat. Commun. **6**, 7957 (2015).
10. D. T. Spencer, T. Drake, T. C. Briles, J. Stone, L. C. Sinclair, C. Fredrick, Q. Li, D. Westly, B. R. Ilic, A. Bluestone, N. Volet, T. Komljenovic, L. Chang, S. H. Lee, D. Y. Oh, M.-G. Suh, K. Y. Yang, M. H. P. Pfeiffer, T. J. Kippenberg, E. Norberg, L. Theogarajan, K. Vahala, N. R. Newbury, K. Srinivasan, J. E. Bowers, S. A. Diddams, and S. B. Papp, Nature **557**, 81 (2018).
11. S. B. Papp, K. Beha, P. Del'Haye, F. Quinlan, H. Lee, K. J. Vahala, and S. A. Diddams, Optica **1**, 10 (2014).
12. P. Marin-Palomo, J. N. Kemal, M. Karpov, A. Kordts, J. Pfeifle, M. H. Pfeiffer, P. Trocha, S. Wolf, V. Brasch, M. H. Anderson, R. Rosenberger, K. Vijayan, W. Freude, T. J. Kippenberg, and C. Koos, Nature **546**, 274 (2017).
13. A. Fülöp, M. Mazur, A. Lorences-Riesgo, Ó. B. Helgason, P.-H. Wang, Y. Xuan, D. E. Leaird, M. Qi, P. A. Andrekson, A. M. Weiner, and V. Torres-Company, Nat. Commun. **9**, 1598 (2018).
14. B. Stern, X. Ji, Y. Okawachi, A. L. Gaeta, and M. Lipson, Nature **562**, 401 (2018).
15. N. G. Pavlov, S. Koptyaev, G. V. Lihachev, A. S. Voloshin, A. S. Gorodnitskiy, M. V. Ryabko, S. V. Polonsky, and M. L. Gorodetsky, Nat. Photonics **12**, 694 (2018).
16. A. S. Raja, A. S. Voloshin, H. Guo, S. E. Agafonova, J. Liu, A. S. Gorodnitskiy, M. Karpov, N. G. Pavlov, E. Lucas, R. R. Galiev, A. E. Shitikov, J. D. Jost, M. L. Gorodetsky, and T. J. Kippenberg, Nat. Commun. **10**, 680 (2019).
17. E. Obrzud, S. Lecomte, and T. Herr, Nat. Photonics **11**, 600 (2017).
18. D. C. Cole, J. R. Stone, M. Erkintalo, K. Y. Yang, X. Yi, K. J. Vahala, and S. B. Papp, Optica **5**, 1304 (2018).
19. C. Joshi, J. K. Jang, K. Luke, X. Ji, S. A. Miller, A. Klenner, Y. Okawachi, M. Lipson, and A. L. Gaeta, Opt. Lett. **41**, 2565 (2016).
20. T. Herr, V. Brasch, J. D. Jost, C. Y. Wang, N. M. Kondratiev, M. L. Gorodetsky, and T. J. Kippenberg, Nat. Photonics **8**, 145 (2014).
21. C. Bao, L. Zhang, A. Matsko, Y. Yan, Z. Zhao, G. Xie, A. M. Agarwal, L. C. Kimerling, J. Michel, L. Maleki, and A. E. Willner, Opt. Lett. **39**, 6126 (2014).
22. X. Xue, P.-H. Wang, Y. Xuan, M. Qi, and A. M. Weiner, Laser Photon. Rev. **11**, 1600276 (2017).
23. V. E. Lobanov, G. Lihachev, and M. L. Gorodetsky, Europhys. Lett. **112**, 54008 (2015).
24. W. Liang, A. A. Savchenkov, V. S. Ilchenko, D. Eliyahu, D. Seidel, A. B. Matsko, and L. Maleki, Opt. Lett. **39**, 2920 (2014).
25. Y. Liu, Y. Xuan, X. Xue, P.-H. Wang, S. Chen, A. J. Metcalf, J. Wang, D. E. Leaird, M. Qi, and A. M. Weiner, Optica **1**, 137 (2014).
26. X. Xue, Y. Xuan, P.-H. Wang, Y. Liu, D. E. Leaird, M. Qi, and A. M. Weiner, Laser Photon. Rev. **9**, L23 (2015).
27. X. Xue, Y. Xuan, Y. Liu, P.-H. Wang, S. Chen, J. Wang, D. E. Leaird, M. Qi, and A. M. Weiner, Nat. Photonics **9**, 594 (2015).
28. J. K. Jang, Y. Okawachi, M. Yu, K. Luke, X. Ji, M. Lipson, and A. L. Gaeta, Opt. Express **24**, 28794 (2016).
29. T. Carmon, H. G. L. Schwefel, L. Yang, M. Oxborrow, A. D. Stone, and K. J. Vahala, Phys. Rev. Lett. **100**, 103905 (2008).
30. S. Ramelow, A. Farsi, S. Clemmen, J. S. Levy, A. R. Johnson, Y. Okawachi, M. R. E. Lamont, M. Lipson, and A. L. Gaeta, Opt. Lett. **39**, 5134 (2014).
31. M. R. E. Lamont, Y. Okawachi, and A. L. Gaeta, Opt. Lett. **38**, 3478 (2013).
32. S. A. Miller, Y. Okawachi, S. Ramelow, K. Luke, A. Dutt, A. Farsi, A. L. Gaeta, and M. Lipson, Opt. Express **23**, 21527 (2015).
33. P. Del'Haye, A. Schliesser, O. Arcizet, T. Wilken, R. Holzwarth, and T. J. Kippenberg, Nature **450**, 1214 (2007).
34. Y. Okawachi, M. Yu, K. Luke, D. O. Carvalho, S. Ramelow, A. Farsi, M. Lipson, and A. L. Gaeta, Opt. Lett. **40**, 5267 (2015).
35. K. E. Webb, J. K. Jang, J. Anthony, S. Coen, M. Erkintalo, and S. G. Murdoch, Opt. Lett. **41**, 277 (2016).
36. X. Gu, M. Kimmel, A. Shreenath, R. Trebino, J. Dudley, S. Coen, and R. Windeler, Opt. Express **11**, 2697 (2003).